Received: 6 July 2022 | Accepted: 25 July 2022

DOI: 10.1111/ahe.12851

Anatomia Histologia Embryologia

WILEY

ORIGINAL ARTICLE

Skull anatomy of the endangered Patagonian huemul deer(*Hippocamelus bisulcus*)

Samuel Núñez-Cook[1,2] | **Fernando Vidal Mugica**[3,4,5,6] | **Paulo Salinas**[2]

[1]Estudiante de Programa de Magíster en Ciencias mención Morfología, Universidad de La Frontera, Temuco, Chile

[2]Laboratory of Animal & Experimental Morphology, Institute of Biology, Pontificia Universidad Católica de Valparaíso, Valparaíso, Chile

[3]Departamento de Ciencias Basicas, Facultad de Ciencias, Universidad Santo Tomas, Temuco, Chile

[4]Fauna Andina, Wildlife Conservation and Management Center, Villarrica, Chile

[5]IUCN, Deer Specialist Group, Apple Valley, Minnesota, USA

[6]IUCN, Conservation Planning Specialist Group, Apple Valley, Minnesota, USA

Correspondence
Paulo Salinas, Laboratory of Animal & Experimental Morphology, Institute of Biology, Pontificia Universidad Católica de Valparaíso, Av. Universidad 330, Valparaíso, Chile.
Email: paulo.salinas@pucv.cl

Abstract

Studies of the normal skull anatomy of the Patagonian Huemul deer are scarce. Currently, the findings of bone lesions in the skull associated with metabolic imbalances are frequent in the literature. The objective of this study was to provide anatomical and morphometric data of the cranium and facies including a morphofunctional interpretation as a reference for clinical, ecomorphological and educational purposes. Five skulls were described, measured, scanned and digitally reconstructed. The presence of a caudal projection of the vomer bone, the absence of the facial tubercle and thin bones forming the cranial cavity were observed. Linear measurements allowed the skull to be classified as dolichocephalic, hyperlepten and ultra-dolichocranial. In conclusion, the Patagonian Huemul has a long head, an extremely long skull and a very narrow face. The thickness of the bones that made up the walls of the cranial cavity suggests chronic metabolic imbalances in response to mineral deficiency. The anatomical and morphometric data obtained in this study strongly emphasizes the relevance of considering the implementation of such management policies that aim at promoting an optimal nutritional context.

KEYWORDS
cranium, deer, facies, huemul, osteology, skull

1 | INTRODUCTION

The Patagonian huemul deer (*Hippocamelus bisulcus*) is considered an endangered by the International Union for the Conservation of Nature (Black-Decima et al., 2016). Currently there is an approximate population of 1500 specimens distributed in Chile and Argentina (Riquelme et al., 2018). We previously published about the anatomy of the appendicular skeleton in the Patagonian huemul deer (Salinas, Arenas-Caro, et al., 2020, Salinas, Núñez-Cook, et al., 2020). The reported background revealed bone characteristics similar to sheep and goats, suggesting the presence of powerful flexor muscles in the scapulohumeral and elbow joints, useful for cushioning jumps and the presence of powerful extensor muscles in the coxofemoral, femorotibial and tarsal joints, useful for walking, running and propulsion. This information is relevant from the conservation point of view. Further, it contributes to the understanding of the current health context of the Patagonian huemul deer, where bone and immune pathologies resulting from the micronutrients deficiency affecting bone metabolism, contribute to the significant reduction in the huemul population (Escobar et al., 2020; Flueck, 2015, 2018, 2020; Flueck & Smith-Flueck, 2017, 2018, 2020; Smith-Flueck et al., 2018).

Prior descriptions of the skull anatomy of the Patagonian huemul deer have limited, since they have been approached from a comparative and evolutionary perspective with other cervids, without emphasizing morphometric or anatomical details typical of the species (Cabrera, 1941; Heckeberg, 2020; Merino et al., 2005; Wemmer & Wilson, 1987). Data on osteopathy was inspired by the need for a circumstantial improvement in vivo diagnoses given the morbidity reported in clinical case that involve the head (Flueck, 2018; Flueck & Smith-Flueck, 2008, 2017, 2020). Such osteopathies affect the ability to avoid predators, reduce their feeding efficiency, alter the development of their ecology and, therefore, prevent population

recovery (Flueck, 2018; Flueck & Smith-Flueck, 2017). Considering its endangered status (IUCN red list, Black-Decima et al., 2016) knowledge on skull anatomy of the Patagonian huemul deer is important for successful surgical procedures (Audisio et al., 2011; Clarke & Trim, 2013; Hall et al., 2000). It is essential to generate new knowledge of a species that presents reduced population numbers, even though multiple efforts and binational projects have been implemented to attempt to reverse its endangered species status. Our results will be a contribution to biological understanding, conservation medicine, surgery and clinical medicine from a morphological perspective. The aim of this study was to provide detailed anatomical and morphometric data on bones of the skulls of the Patagonian huemul deer as a reference for teaching, clinical and ecomorphological uses.

2 | MATERIALS AND METHODS

This study was conducted in the Laboratory of Animal and Experimental Morphology of the Institute of Biology at the Pontificia Universidad Católica de Valparaíso. A descriptive, cross-sectional design was performed. Five (n_{total} = 5; Male = 4; Female = 1) skulls of Patagonian huemul deer obtained by exhumation in Region of La Araucanía (Fauna Andina; Villarrica 39°16′00″S, 72°13′00″W; 227 m.a.s.l., Chile) and in Region of Aysén del General Carlos Ibáñez del Campo (Lake Paloma 45°55′00.7″S 72°08′34.3″W and Cerro Castillo 46°03′00″S 72°11′00″O; Chile) were used. Given the great heritage value of the specimens handling, transportation and storage were done according to Simmons and Muñoz-Saba (2005). Further, handling and transportation were done within the framework of Resolution (N° 1.490) of the Chilean Agricultural and Livestock Service of 22nd December 2003.

Cranium and facies anatomy were studied, with special emphasis on the description of the osseous elevations and depressions. The following were assessed: (i) linear variables such as: total neurocranial length (NL), viscerocranial length (VL), vertical orbital diameter (VOD), horizontal orbital diameter (HOD), total neurocranial width (TWN) and others (Gündemir et al., 2020; Keneisenuo et al., 2021; Figure 1), (ii) craniometric indices such as: Total Cephalic Index (TCI: [TWS/TSL]*100) (Sañudo, 2009), Facial Index (FI: [WZA*100]/LV) (Sañudo, 2009), Cranial Index (CI: [TWN*100]/LV) (Sañudo, 2009) and Mandibular Index (MI: [TJH*100]/TJL) (Krenzer, 2006) and (iii) bone thickness, for which 12 points of surgical and anatomical interest were considered (Sandoval et al., 2016). A 16MP Canon® EOS Rebel T3i digital camera was used to capture images. For the observation of the translucence of the skull, a light source was inserted into the cranial cavity. In addition, an analysis of surfaces and cavities was done using computed tomography (CT scan; Mx8000 IDT 16, Philips Medical Systems DMC GmbH, Hamburg, Germany). Cross-sectional images were acquired according to Brinkschulte et al. (2013). The image analysis and 3D reconstruction were done using the Slicer software v. 4.11.2021026 (Fedorov et al., 2012) with the SlicerMorph extension (Rolfe et al., 2021) for DICOM

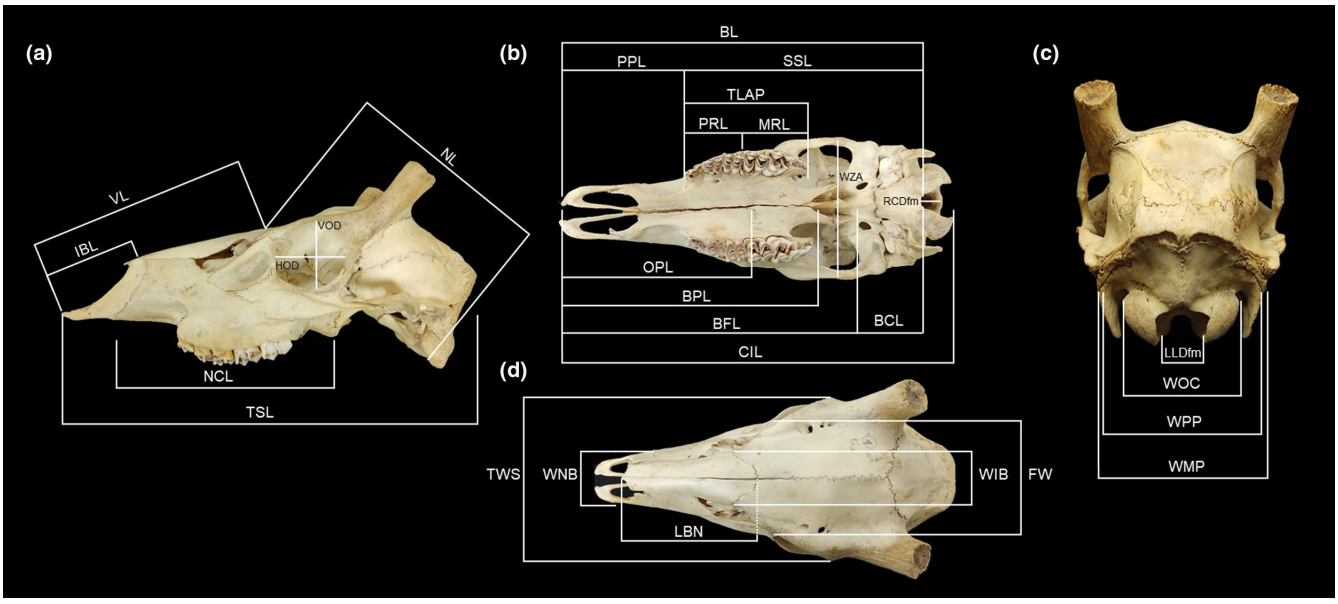

FIGURE 1 Linear measurements in the skull of Patagonian Huemul deer. (a) lateral view: total skull length (TSL), neurocranial length (NL), viscerocranial length (VL), nasal cavity length (NCL), horizontal orbit diameter (HOD), vertical orbit diameter (VOD), incisor bone length (IBL). (b) ventral view: condyle-incisor length (CIL), basal length (BL), short skull length (SSL), premolar to prosthion length (PPL), basecranial length (BCL), basefacial length (BFL), bony palatal length (BPL), oral palatal length (OPL), total length of alveolar process (TLAP), premolar row length (PRL), molar row length (MRL), width between zygomatic arches (WZA), rostrocaudal diameter of foramen magnum (RCDfm). (c) caudal view: laterolateral diameter of foramen magnum (LLDfm), width between occipital condyles (WOC), width between paraoccipital processes (WPP), width between mastoid processes (WMP). (d) dorsal view: length of nasal bone (LBN), width between nasal bones (WNB), length between incisor bones (WIB), total skull width (TWS), facial width (FW)

files. The terminology used was based on the 6th edition (revised) of the Nomina Anatomica Veterinaria (NAV) (ICVGAN, 2017). The quantitative data were organized in Excel tables (Microsoft Corporation, 2018) according to sex, expressed by means of descriptive statistics such as averages and standard deviation. The craniometric indices were expressed as percentages.

3 | RESULTS

3.1 | Cranium

The data and images that supports the findings of this study are available in the supplementary material of this article. The bones that formed the walls of the cranial cavity (*Cavum cranii*) were as follows: occipital (*Osoccipitale*), parietal (*Osparietale*), basisphenoid (*Osbasisphenoidale*), presphenoid (*Ospresphenoidale*), ethmoid (*Osethmoidale*), frontal (*Osfrontale*), temporal (*Ostemporale*) and pterygoid (*Ospterygoideum*) (Figures 2 and 3).

The occipital bone formed part of the ventrocaudal wall of the skull, emphasizing a wide and circular foramen magnum. The dorsal margin of the foramen magnum presented two well-defined nuchal tubercles. The outer surface of the basilar portion presented with two muscular tubercles. On the median plane, a longitudinal bone line was observed that continued even to the body of the basisphenoid. On the inner surface, there were smooth surface medullary and pontine impressions, concave and well defined. Rostrally, it articulated with the basisphenoid bone by means of a distinguishable synchondrosis spheno-occipitalis on both surfaces of the skull. The lateral portion articulated by sutures with the temporal bone. The paracondylar processes presented the same height as the occipital condyles. The ventral condylar fossa was deep and presented the hypoglossal canal on its lateral wall. The condylar fossa had a porous surface. The inner surface of the foramen magnum presented the opening of hypoglossal canal and the condylar canal. The intrajugular process was observed from both surfaces. With respect to the squama, the wedge-shaped external occipital protuberance and a sharp nuchal line were noteworthy. The temporal line projected latero-rostrally. Dorsally and ventrally to the external occipital protuberance, a smooth rectangular area and the external occipital crest, respectively, were observed. The inner surface presented the impression of the vermis, flanked by the internal occipital crests and the impressions of the cerebellar lobes. In addition, a groove of the transverse sinus was present, forming an arch. The apex of which was situated in the medial portion of the occipitoparietal suture (Figure 2).

The basisphenoid bone had a smooth outer surface and a foramen for the craniopharyngeal canal. The body had a trapezoid shape, a smooth outer surface and the foramen for the craniopharyngeal canal. The inner surface presented a well-defined sella turcica and carotid groove. The dorsum had the shape of a widened ramp similar to an obcordate leaf. In some specimens, the hypophyseal fossa presented a foramen. The caudal clinoid processes were scarcely evident. The wings presented a foramen ovale and a ventromedial canal that went across the body of the basisphenoid. The temporal surface articulated with the temporal bone. The maxillary and orbital faces were smooth and rough, respectively. The cerebral surface, which articulated with the parietal and temporal bones, presented the pyriform fossa. The smooth, flat surfaced pterygoid process was oriented rostroventrally, accompanying the palatine (*Os palatinum*) and pterygoid bones, forming the lateral wall of the choana (Figure 4).

The presphenoid bone was located centrally and rostrally to the body of the basisphenoid bone. The inner surfaces of the body and wing formed the bone wall of the rostral cranial fossa. The outer surface of the body articulated with the vomer by means of the sphenoid crest near the chiasmatic groove, forming part of the dorsal wall of the choana. The inner surface presented the chiasmatic groove and a long, smooth jugum sphenoidale. The outer surface of the wing formed part of the orbit by means of a thin plate, which articulated with the lacrimal bone (*Oslacrimale*; Figure S12). The base housed the optic canal.

The pterygoid bone was located medial to the perpendicular plate of the palatine and the pterygoid process of the basisphenoid bone. It was a triangular shaped, with the base oriented dorsally. Its lateral surface articulated with the pterygoid process and the perpendicular plate of the palatine. Its medial surface formed part of the lateral wall of the choana. The pterygoid hamulus protruded ventrally and was observed from both surfaces (Figure 4).

The temporal bone was prominent. The petrous part was rough and articulated with the paracondylar process of the occipital bone. The occipital surface presented a robust mastoid process. The rostral surface, had a smooth surface and presented a small canal of the greater petrosal nerve, highlighting the impression of the trigeminal nerve. Rostroventrally the apex presented two bone projections. On the medial surface, the internal acoustic meatus and cerebellar fossa were observed. The convergence between the rostral and medial surfaces was at the crest of the petrous part, which in its caudal portion housed a space for the transverse sinus. The ventral margin was irregularly shaped, constituting the jugular notch. Part of the ventral surface was covered by the tympanic part, surrounding a cylindrical styloid process. The stylomastoid foramen was found between the styloid process and the mastoid process. With respect to the tympanic part, the tympanic ring was U-shaped. The sheath of the styloid process was sharp. Medially to the tympanic ring, a medium-sized bulla tympanica was observed. In addition, the muscle process was oriented medially with several peaks. The parietal margin of the squamous part articulated with the parietal bone, occipital bone (as the occipital process via a suture) and the petrous part of the temporal bone (via the mastoid process). The sphenoidal margin articulated with the basisphenoid bone. The temporal surface articulated caudally with the mastoid process by means of the supramastoid crest. A concave zygomatic process projected rostrolaterally, articulating with the temporal process of the zygomatic bone, forming to the zygomatic arch. The mandibular fossa was pyriform and flanked by the articular tubercle and the retroarticular process.

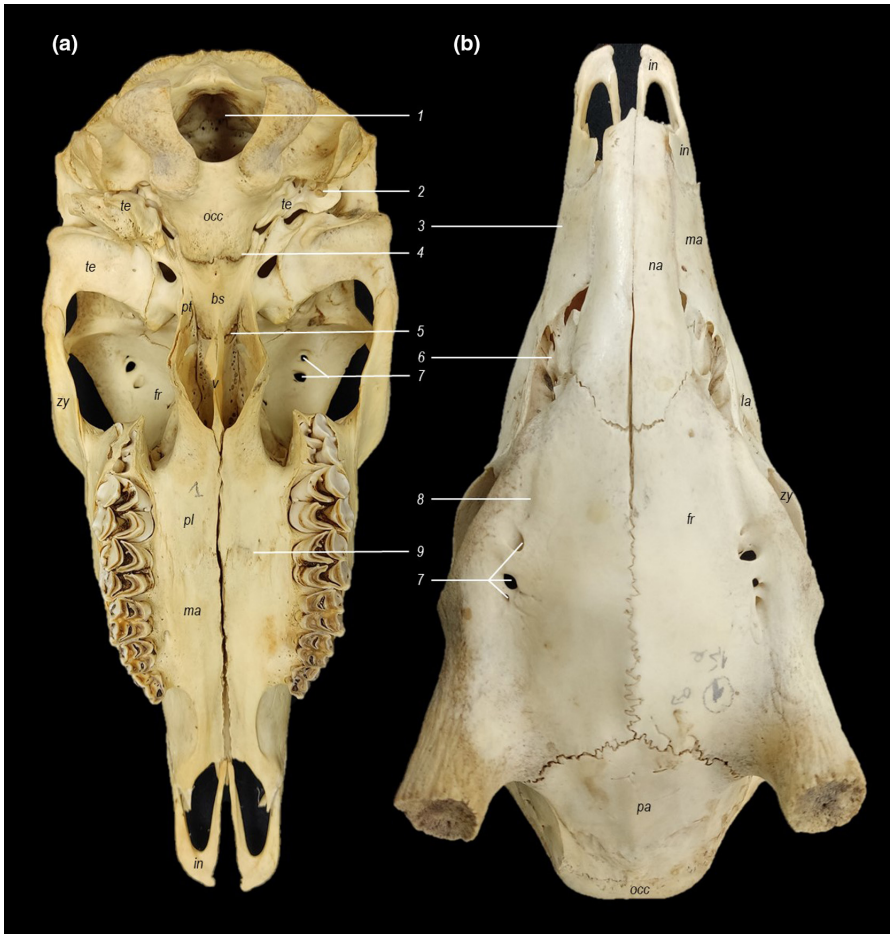

FIGURE 2 Skull and face of Patagonian Huemul deer. (a) ventral view, (b) dorsal view. Parietal bone (pa); frontal bone (fr); temporal bone (te); basisphenoid bone (bs); zygomatic bone (zy); lacrimal bone (la); palatine bone (pl), pterygoid bone (pt); nasal bone (na); maxilla (ma); vomer (v); occipital bone (occ); incisive bone (in). 1, foramen magnum. 2, styloid process. 3, body of the maxilla. 4, sphenoccipital synchondrosis. 5, intersphenoid synchondrosis. 6, nasolacrimal fissure. 7, supraorbital foramina. 8, supraorbital groove. 9, transverse palatine suture

Dorsal to the external acoustic meatus was the retrotympanic process and the retroarticular foramen, which on their respective bases presented foramina that connected the outer surface to the cranial cavity (Figure S3).

The parietal bone presented a flat and convex outer surface. It articulated with the frontal, temporal and occipital bones. The sphenoid and mastoid angles were clearly distinguishable. The inner surface presented a tentorial process, which rose rostrally, accompanying the sulcus of the dorsal sagittal sinus. The rest of the surface presented *impressiones digitatae* and *vascular sulci*. The outer surface presented a prominent parietal tubercle and a double temporal line (Figure S6).

The frontal bone presented a bony prominence between the antlers. The frontal squama, in general, had a smooth surface. A supraorbital groove was observed, accompanied by three supraorbital foramina. The zygomatic process of the frontal bone was articulated with the zygomatic bone by the frontozygomatic suture. The inner surface presented impressionesdigitatae and vascular sulci. It was part of the wing of the presphenoid bone, forming a space that gave rise to the venous sinus of the dura mater. The temporal surface formed part of the rostral portion of the temporal fossa. The nasal part had a smooth surface. In the nasal margin, an arrowhead-shaped notch was observed, which articulated with the nasal bones via the frontonasal suture. The orbital part comprised the dorsomedial wall of the orbit, highlighting the presence of the ethmoid foramen (near the sphenofrontal suture) and a trochlear fovea (Figure S12). The frontal bone evidenced sexual dimorphism; males presented cylindrical outgrowths that are known as pedicles. They constitute paired frontal processus from which the antlers are grown and cast. It presented a rough surface, characterized by the presence of numerous grooves in a caudodorsal direction. By contrast, females presented a lateral bone projection that continued caudally from the base of the zygomatic process (Figure 3).

The ethmoid bone presented a crista galli. It was flanked by two concave fossae and by a uniform row of cribriform foramina. The perpendicular plate projected ventrally from the cribriform plate, articulating with the crest of the vomer and forming the bony nasal septum. The orbital, tectorial and basal plates formed a thin and sinuous bone tube. The tectorial plate was oriented toward the frontal and nasal bones, forming a roof over the ethmoid labyrinth. Its lateral portion was thinner that the medial portion. The basal plate represented a bone base for the ethmoid labyrinth (Figure S6).

3.2 | Facies

The bones of the facies were as follows: vomer (*vomer*), nasal (*os nasale*), lacrimal, maxilla (*maxilla*), ventral nasal concha (*os conchae nasalis ventralis*), incisive (*osincisivum*), palatine and zygomatic (Figures 2 and 3).

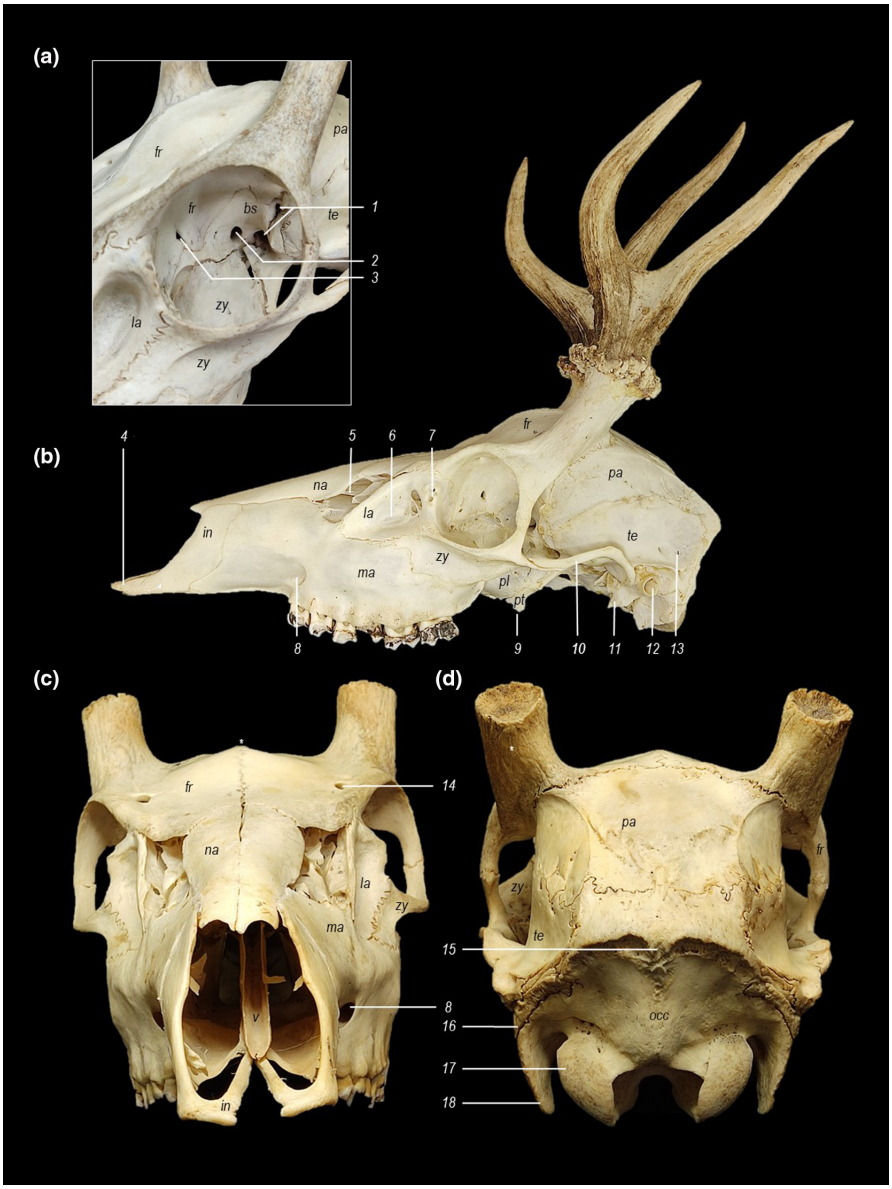

FIGURE 3 Skull and face of Patagonian Huemul deer. (a) Orbit, (b) lateral view, (c) rostral view, (d) caudal view. Parietal bone (pa); frontal bone (fr); temporal bone (te); basisphenoid bone (bs); zygomatic bone (zy); lacrimal bone (la); palatine bone (pl), pterygoid bone (pt); nasal bone (na); maxilla (ma); vomer (v); occipital bone (occ); incisive bone (in). 1, foramen orbitorotundum. 2, optic canal. 3, ethmoid foramen. 4, body of the incisive bone. 5, nasolacrimal fissure. 6, external lacrimal fossa. 7, lacrimal foramina. 8, infraorbital foramen. 9, pterygoid hamulus. 10, zygomatic process of the temporal bone. 11, sheath of the styloid process. 12, external acoustic meatus. 13, foramen of the temporal scale. 14, supraorbital foramen. 15, external occipital protuberance. 16, mastoid process. 17, occipital condyle. 18, paracondylar process. *: pedicle (unnamed in NAV)

The vomer formed part of the caudal portion of the nasal septum. On the floor of the nasal cavity, it articulated with the palatine (caudal portion), maxilla (medial portion) and incisive (rostral portion) bones. It presented a septal groove inclined rostroventrally. The vomerine crest projected caudodorsally, leaving a free space between the choana and the body of the basisphenoid bone. The vomerine wing presented a series of foramina, giving it a cribriform appearance (Figure S5).

The nasal bone articulated with the frontal (by means of the frontonasal suture), contralateral nasal (by means of the internasal suture) and maxilla (by means of the flat nasomaxillary suture) bones. Its outer surface was smooth and slightly convex. Its inner surface was smooth and concave; in its caudo-lateral portion the ethmoid crest was observed with an incomplete oval shape. Rostrally, it presented two sharp bone eminences. The medial one was longer and was close to the septal process (Figure 3).

The lacrimal bone articulated with the frontal, zygomatic and maxilla bones by means of dentate sutures (frontolacrimal, lacrimozygomatic and lacrimomaxillary sutures, respectively) and a small portion with the palatine and sphenoid bones. It had three faces: orbital, facial and nasal. The first two was bound to each other by supra- and infraorbital margins, in which two lacrimal foramina were observed. On the orbital face, the opening of the lacrimal canal and sac was observed. Caudomedially to this, the fossa of the ventral muscle of the eyeball was observed. The ventral wall was thin and being part of the lacrimal bulla was the caudal boundary of the maxillary sinus. The nasal face had thin walls, which also formed part of the walls of the maxillary and lacrimal sinuses (Figure S12).

The maxilla articulated with all the facial bones. The body presented a smooth facial surface with ample convexities and alveolar eminences. At the level of the second premolar was the infraorbital foramen that corresponded to the opening of the infraorbital canal, which began in the maxillary foramen on the pterygopalatine surface. From the infraorbital channel, the incisive canal projected, which ended in the incisive bone. On the nasal surface, a thin and

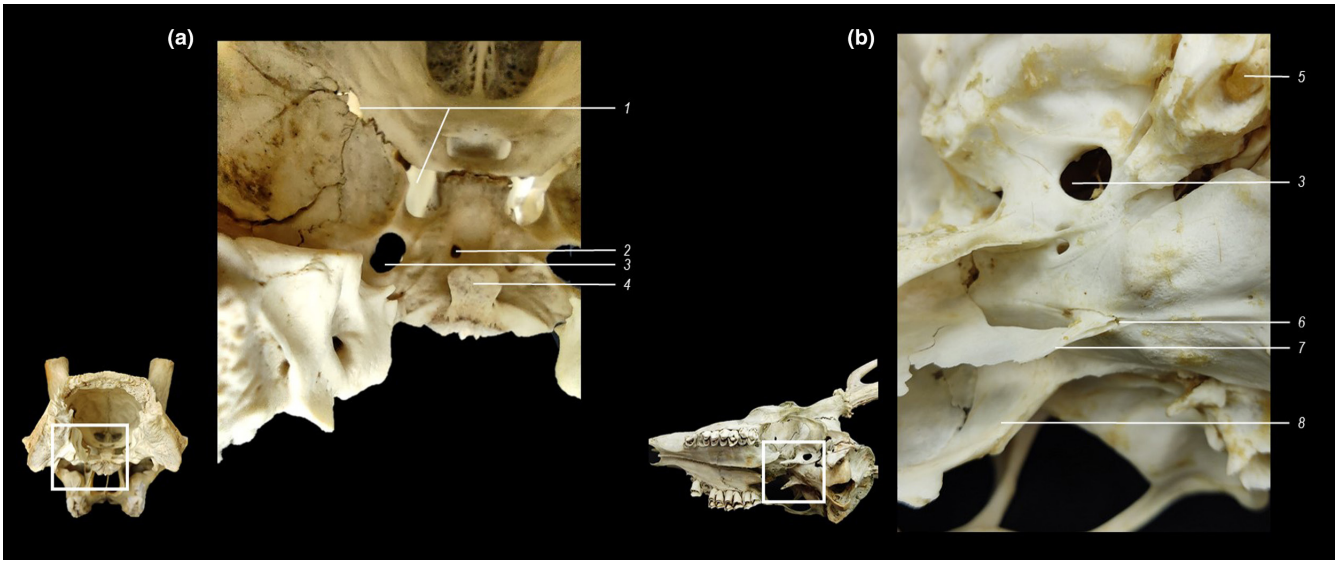

FIGURE 4 Middle area of the base of the skull of the Patagonian Huemul deer. (a) Internal view. (b) external view. 1. foramen orbitorotundum, 2. Internal opening of the craniopharyngeal canal, 3. Foramen ovale, 4. dorsum sella turcica, 5. styloid process, 6. external opening of the craniopharyngeal canal, 7. caudal projection of the vomerine crest, 8. medial surface of the pterygoid bone

sharp conchal crest was worthy of note, accompanied by the maxillary hiatus, which communicated dorsally with the maxillary sinus. Ventrally to the conchal crest, the lacrimal groove and canal were observed. The zygomatic process articulated with the zygomatic and lacrimal bones via the zygomaticomaxillary and lacrimomaxillary sutures, respectively, both dentate. The palatine process projected medially from the alveolar processes to articulate with the contralateral maxilla (median palatine suture, flat type). Caudally, it articulated with the palatine bone (transverse suture, bevelled type). Rostrally, it formed with the caudal part of the palatine fissure. Between the median palatine suture and the teeth, the palatine groove stood out, which ended at the major palatine foramen. This was located near the transverse palatine suture. The nasal surface presented a nasal crest. The alveolar process presented three alveoli for the premolars and three molars; in addition, each presented with one to three interradicular septa (Figure 3).

From the incisive bone, the labial and palatine surfaces of the body presented smooth surfaces and a rostromedial projection, which formed part of the rostral portion of the palatine fissure. A curved palatine process articulated with the palatine process of maxilla and with the ventral portion of the vomer. In addition, it formed the medial portion of the palatine fissure. The palatine process presented a wide interincisive fissure. The nasal process was flat, wide, curved and presented a rounded bone eminence. It articulated with the maxilla by means of the maxilloincisive suture (Figure 2; Figure S8).

The perpendicular plate of the palatine bone articulated with the presphenoid, pterygoid and ethmoid bones. Both its nasal and maxillary surfaces had a smooth surface. In the latter, the sphenopalatine foramen or notch was observed. Ventrally to this last one, the smaller caudal palatine foramen was located. The horizontal plate presented a blunt caudal nasal thorn in its caudal half. On its nasal surface it presented a nasal crest. On the palatine surface, it presented a major palatine foramen. The minor palatine foramina were small (Figure 2; Figure S8).

The zygomatic bone, sigmoid-shaped, formed part of the orbit and the lateral and caudal walls of the maxillary sinus. It articulated with the maxilla, frontal, lacrimal and temporal bones via the zygomaticomaxillary, frontozygomatic, lacrimozygomatic and temporozygomatic bones, respectively. The first two were flat and the last two were bevelled. The lateral surface had a smooth surface and in most of the skulls studied it presented a ventral foramen in the middle of the ventral wall of the orbit. The orbital surface was concave and smooth. The temporal process of the zygomatic bone was curved and presented a concave dorsal margin. It articulated with the zygomatic process of the temporal bone forming the zygomatic arch. The frontal process articulated with the zygomatic process of the frontal bone by means of a dentate suture, constituting the supraorbital margin.

The lacerate and jugular foramina were formed by the occipital, basisphenoid and temporal bones (Figure 2). The two were connected by the tympano-occipital fissure. The margins of the lacerate foramen were as follows: the body of the basisphenoid bone (rostral), temporal bone (cauda), wing of the basisphenoid bone (lateral) and basal portion of the occipital bone (medial). The margins of the jugular foramen were as follows: temporal bone (dorsal), lateral portion of the occipital bone (ventral), temporal bone (lateral) and lateral portion of the occipital bone (medial). The temporal fossa was formed by the parietal, temporal, frontal and basisphenoid bones. Its boundaries were as follows: temporal line (dorsal boundary), nuchal crest (caudal boundary), caudal margin of the frontal process of the zygomatic bone and the zygomatic of the frontal bone (rostral boundary), supramastoid crest and zygomatic arch (lateral boundary). Its walls were as follows: parietal bone (dorsomedial), the

squama of the temporal bone (dorsoventral), wing of the basisphenoid bone (rostromedial) and squama of the temporal bone (ventral wall). In the female skull, more openings were noted, collateral to the temporal meatus and parietotemporal foramina throughout the squamous suture. The pterygopalatine fossa was formed by the rostral portion of the orbit and the palatine, lacrimal and maxilla bones. Its boundaries were the virtual floor of the orbit (dorsal) and the pterygoid fossa (caudal). Its walls were formed by the maxilla and perpendicular plate of the palatine bone (rostral), maxillary tubercle and a portion of the lacrimal bone associated with the maxillary sinus (lateral) and perpendicular plate of the palatine bone (medial). The maxillary, caudal palatine (opening of the palatine canal) and sphenopalatine foramina were present in the deepest portion of the pterygopalatine fossa. Generally, the latter was made up exclusively by the palatine bone, whereas in two skulls the wing of the presphenoid bone represented its dorsal margin. The cranial cavity presented impressionesdigitatae and the groove of the dorsal sagittal sinus (midline) on its inner surface. The rostral cranial fossa (from the cribriform plate of the ethmoid bone to the orbitosphenoidal crest), the middle cranial fossa (from the orbitosphenoidal crest to the back of the sella turcica) and the caudal cranial fossa (from the back of the sella turcica to the intercondylar notch) presented easily distinguishable boundaries (Figure 5). The skull weights and volumes of the cranial cavity are listed in Table 1.

The orbit was formed by the frontal, lacrimal, zygomatic, palatine, presphenoid, basisphenoid and parietal bones (Figure 3). It was oriented rostrolaterally at a 65° angle to the frontal plane. The dorsal wall was constituted mainly by the orbital surface of the frontal bone, where there was evidence of the trochlear fovea and the supraorbital canals, with these communicating with the dorsal surface of the skull. The medial wall is represented by the wing of the presphenoid bone, the orbital surface of the frontal bone and by the perpendicular plate of the palatine bone, highlighting the ethmoid foramen. Close to the orbital apex, the optical canal communicated with the middle cranial fossa. The lateral wall was made up of the zygomatic process of the frontal bone and the frontal process of the zygomatic bone. The ventral wall, constituted by the orbital surface of the zygomatic bone, presented rostrolateral structures such as: the fossa of the lacrimal sac, the opening of the lacrimal canal, the fossa of the ventral muscle of the eyeball and lacrimal bulla. The base was open and bounded by the orbital margins. The apex was formed by the wing of the presphenoid and basisphenoid bones together with part of the parietal bone, emphasizing the foramen orbitorotundum located caudolaterally to the opening of the optical canal and communicating with the middle cranial fossa. It presented supraorbital and infraorbital margins that jointly gave it a circular shape. The horizontal diameter of which was 4.20 and 4.06 cm in females and males, respectively. On the rostral plane, the presence of two lacrimal foramina stood out.

The *foramen orbitorotundum* was formed by the wings of the basisphenoid and presphenoid bones, in addition to smaller portions of the frontal and parietal bones. It presented ventral (small) and dorsal (great) portions. The ventral portion was flanked by the body (middle) and wing (lateral) of the basisphenoid bone and, in addition, by the wing of the presphenoid bone (dorsal). The dorsal portion was formed by the frontal bone (dorsal), parietal bone (ventral) and wing of the basisphenoid bone (rostroventral). Ventrally a vertex was formed with the wing of the basisphenoid bone (Figures 3 and 4). The results of the linear measurements are in Table 2. The craniometric indices made it possible to describe the skull of the Patagonian huemul deer as: dolichocephalic, hyperleptene and ultra-dolichocranial (Table 3). The results of the skull bone thickness appear in Table 4 and Figure 6 demonstrates the translucency of the skulls studied.

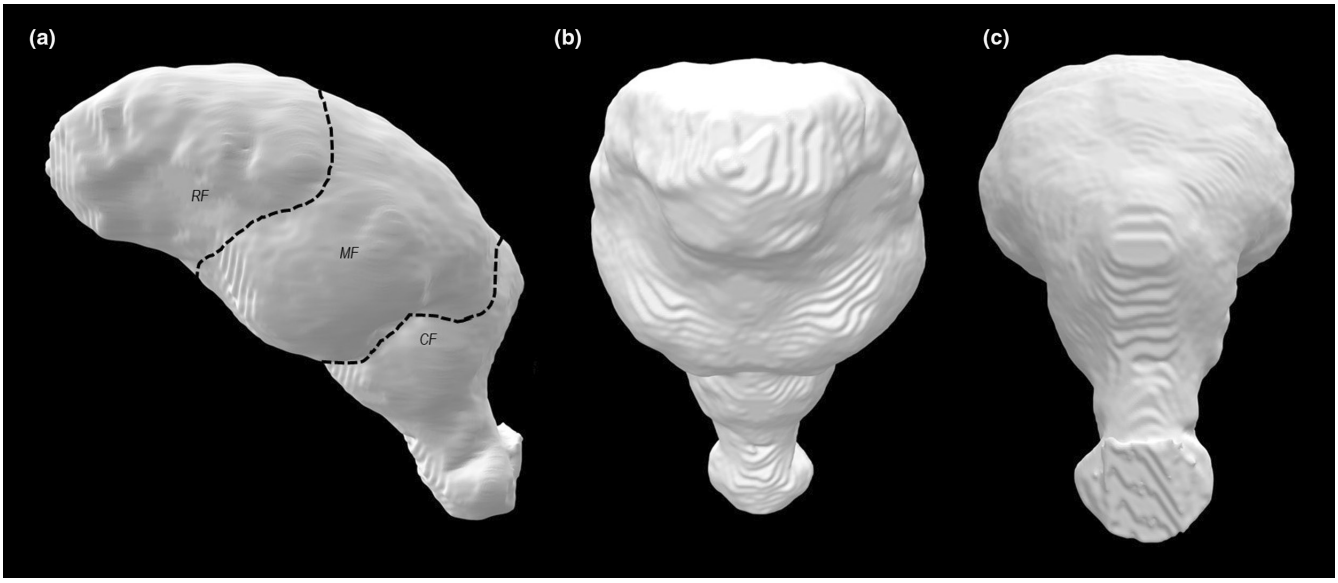

FIGURE 5 3D reconstruction of cranial cavity of Patagonian Huemul deer. (a) lateral view. (b) rostral view. (c) caudal view. Rostral cranial fossa (RF), middle cranial fossa (MF), caudal cranial fossa (CF)

TABLE 1 Weight of the skull and cranial cavity volume in Patagonian Huemul deer ($n = 5$)

ID	Age (years)	Weight (g)	Volume (cm^3)
1	1.5	302	159.8
2	3	661	183.3
3	4	484	201.9
4	7	306	176.0
5	2	489	201.9

TABLE 3 Craniometric indices (%) in the skull of Patagonian Huemul deer ($n = 3$)

Index	Mean ± *SD*	Range (min. Max.)
Total cephalic index	39.9 ± 0.8	39.0–40.5
Facial index	71.5 ± 6.1	67.9–78.5
Cranial index	47.1 ± 4.6	44.5–52.5
Mandibular index	45.2 ± 2.3	43.0–47.5

4 | DISCUSSION

To the best of our knowledge, the present study is the first detailed anatomical description of the skull of Patagonian huemul deer. The descriptions and linear measurements reported in this study are a compilation of relevant scientific information, permitting its identification and differentiation from other species, contemporary and extinct (Castañeda et al., 2016; Castaños, 2017; Onuk et al., 2013; Von den Driesch, 1976; Yahaya et al., 2011). Although we discussed and compared the bone findings observed in the Patagonian huemul deer with domestic animals, we did so from a morphological perspective considering that they are animals of a similar body size and in no case from an ecological or evolutionary perspective. Given that the shape of the cranium and facies varies among species, these data will (i) facilitate the identification of skulls and/or species in paleontological studies based on structural and geographic criteria, (ii) improve the criteria and surgical approaches of the skull and in particular (iii) improve the historical, ecological and evolutionary understanding of the Patagonian huemul deer (Escobar et al., 2020; Flueck & Smith-Flueck, 2011, 2020; Iriarte et al., 2017; Smith-Flueck et al., 2018).

4.1 | Differentiating characteristics of the skull

According to the craniocephalic indices, it was possible to classify the Patagonian huemul deer as an animal with an elongated head, that presents an extremely elongated skull and a very narrow face, typical of animals whose diet is based on the consumption of highly digestible plant matter with concentrated minerals (Iriarte et al., 2017). This definition applies to animals of similar build and size that share a habitat with the Patagonian huemul deer, like sheep and goats. Consequently, some reported bone eminences in this study are useful as criteria for identification and differentiation of species or skeletons (Coacalla et al., 2021; Onuk et al., 2013). Such is the case of the tentorial process of the parietal bone. It is a bony eminence

TABLE 2 Linear measurements (mean ± *SD*; cm) in the skull of Patagonian Huemul deer

Variable	Male ($n = 4$)	Female ($n = 1$)	Total ($n = 5$)
TSL	27.7 ± 1.0	29.4	28.3 ± 1.2
CIL	26.2 ± 1.1	27.0	26.5 ± 0.9
BL	24.6 ± 1.2	25.0	24.7 ± 0.9
SSL	15.6 ± 0.7	16.7	15.8 ± 0.7
PPL	8.8 ± 0.6	9.0	8.8 ± 0.4
BCL	5.5 ± 0.2	5.7	5.5 ± 0.2
BFL	19.7 ± 1.1	21.1	20.2 ± 1.1
NL	12.9 ± 0.5	9.1	12.4 ± 1.8
VL	14.6 ± 0.6	16.4	15.2 ± 1.1
WNB	9.8 ± 1.0	11.7	10.2 ± 1.2
NCL	14.4 ± 0.9	16.1	14.8 ± 1.1
BPL	16.9 ± 0.9	18.0	17.2 ± 0.9
OPL	12.8 ± 0.2	13.3	12.9 ± 0.4
IBL	7.1 ± 0.4	8.0	7.4 ± 0.6
TLAP	8.3 ± 0.6	7.1	8.1 ± 0.7
MRL	4.9 ± 0.3	4.3	4.8 ± 0.4
PRL	3.8 ± 0.3	3.2	3.7 ± 0.4
HOD	4.0 ± 0.1	4.2	4.1 ± 0.1
VOD	4.0 ± 0.1	4.1	4.0 ± 0.1
WMP	8.8 ± 0.1	8.5	8.7 ± 0.9
WOC	5.3 ± 0.2	5.3	5.3 ± 0.2
WPP	7.2 ± 0.5	8.2	7.4 ± 0.6
LLDfm	2.3 ± 0.1	2.3	2.3 ± 0.1
RCDfm	2.2 ± 0.1	2.0	2.2 ± 0.1
WZA	10.5 ± 0.5	11.1	10.6 ± 0.5
LBN	3.6 ± 0.3	3.8	3.7 ± 0.3
WIB	3.3 ± 2.1	7.1	4.0 ± 2.5
TWS	11.3 ± 0.3	11.5	11.4 ± 0.3
FW	8.6 ± 0.4	8.7	8.6 ± 0.4
TWN	11.3 ± 0.3	11.5	11.4 ± 0.3

Total skull length (TSL), condyle-incisor length (CIL), basal length (BL), short skull length (SSL), premolar to prosthion length (PPL), basecranial length (BCL), basefacial length (BFL), neurocranial length (NL), viscerocranial length (VL), width between nasal bones (WNB), nasal cavity length (NCL), bony palatal length (BPL), oral palatal length (OPL), incisor bone length (IBL), total length of alveolar process (TLAP), molar row length (MRL), premolar row length (PRL), horizontal orbit diameter (HOD), vertical orbit diameter (VOD), width between mastoid processes (WMP), width between occipital condyles (WOC), width between paraoccipital processes (WPP), laterolateral diameter of foramen magnum (LLDfm), rostrocaudal diameter of foramen magnum (RCDfm), width between zygomatic arches (WZA), length of nasal bone (LBN), length between incisor bones (WIB), total skull width (TWS), facial width (FW), total width of cranial cavity (TWN).

typical of the Patagonian Huemul deer and Fallow deer (*Damadama*; Pohlmeyer, 1985), which allows us to differentiate them from species such as the roe deer (*Capreolus capreolus*; Onuk et al., 2013), reindeer (*Rangifer tarandus*; Castaños, 2017), red deer (*Cervus elaphus*; Castaños, 2017), pudu (*Pudupuda*; Saldivia & Villegas, 2019) or Peruvian guemal (*Hippocamelus antisensis*; Coacalla et al., 2021). In addition, some bony eminences reported in this study are diagnostic characteristics in cervids and, therefore, are useful for their differentiation in comparative studies with domestic animals since they share a habitat. A case is the presence of lacrimal fossa and two lacrimal foramina (Heckeberg, 2020). The fossa was concave, circumscribed and pyriform shaped (Castaños, 2017; Coacalla et al., 2021; Onuk et al., 2013; Saldivia & Villegas, 2019). In turn, the two lacrimal foramina observed in the Patagonian huemul deer differ from the single foramen reported in domestic ruminants (Nickel et al., 1984). A third case is the caudal projection of the vomerine crest, whose dorsal and concave margin left a wide free space between the vomer bone and the body of the basiesphenoid bone. This free space has not been reported in domestic animals or in studies on the skull in other cervids (Castaños, 2017; Nickel et al., 1984; Onuk et al., 2013; Saldivia & Villegas, 2019) except in the Peruvian guemal (Coacalla et al., 2021), which could be different from genus *Hippocamelus*. A fourth case is the absence of the facial crest and tubercle, typical of domestic ruminants (Nickel et al., 1984).

Given the biomechanical relevance in chewing and gripping foods, the absence of robust bone eminences such as the facial crest and tubercle (and the variability observed among ruminants) could be a differentiating biomechanical aspect associated with the insertion of powerful masticatory muscles, mastication and rumination (Clauss et al., 2008; Mateo & Sánchez, 2016). The explanation for the absence of these bone eminences and consequently for the shape of the masseter muscle could be in the nature and trophic ecology of the Patagonian huemul deer (Clauss et al., 2008; Escobar et al., 2020; Iriarte et al., 2017; Mateo & Sánchez, 2016). On the other hand, some bone characteristics that the huemul shares with other cervids (non-domestic ruminants; Coacalla et al., 2021; Onuk et al., 2013) are: the relative latero-caudal direction of the external acoustic pore, the location of the styloid process (between the paracondylar process and the bulla tympanica) and the visibility of the petrous part of the temporal bone.

TABLE 4 Skull bone thickness (mean ± *SD*; cm) of the Patagonian Huemul deer

Variable	Males ($n = 4$)	Females ($n = 1$)	Total ($n = 5$)
TM	0.2 ± 0.1	0.2	0.2 ± 0.1
TF	0.9 ± 0.2	0.8	0.9 ± 0.2
TN	0.1 ± 0.0	0.1	0.1 ± 0.0
TDO	0.7 ± 0.7	0.4	0.6 ± 0.7
TVO	0.2 ± 0.1	0.2	0.2 ± 0.0
TCO	0.3 ± 0.1	0.3	0.3 ± 0.1
TZA	0.4 ± 0.0	0.4	0.4 ± 0.0
TC	0.3 ± 0.1	0.2	0.3 ± 0.1
TP	0.5 ± 0.2	0.3	0.4 ± 0.2
TFMd	0.6 ± 0.1	0.7	0.6 ± 0.1
TFMv	0.7 ± 0.4	0.4	0.6 ± 0.3
TT	0.6 ± 0.1	0.8	0.6 ± 0.2

Notes: Lateral face of maxilla at level of first molar (TM), middle of frontal suture (TF), rostral margin of nasal bone (TN), dorsal margin of orbit (TDO), ventral margin of orbit (TVO), caudal margin of orbit (TCO), zygomatic arch (TZA), lateral margin of the choana (TC), centre of the parietal bone (TP), dorsal margin of the foramen magnum (TFMd), ventral margin of the foramen magnum (TFMv) and rostral margin of the temporal scale (TT).

4.2 | Structures of clinical-surgical importance in the head and face

The presentation of a foramen in the hypophyseal fossa near the spheno-occipital synchondrosis suggests the presence of a ventral opening for the craniopharyngeal canal present during the foetal stage. This finding has been described in rabbits (*Oryctolagus cuniculus*) and other lagomorphs (Arcos, 2021; Núñez, 2018). It characterized for communicating the hypophyseal fossa with an internal space in the body of the basisphenoids bone, which is cut cross-sectionally by a canal. We hypothesized that the foramen in the pituitary fossa was the bony portal of entry for the passage of the pituitary blood vessels. This finding has not been reported in other cervids. The persistence of the craniopharyngeal canal during adulthood has been associated with malformations in domestic cats (*Felis silvestris catus*) diagnosed with hypophyseal dwarfism (Silvestrini et al., 2008). It is

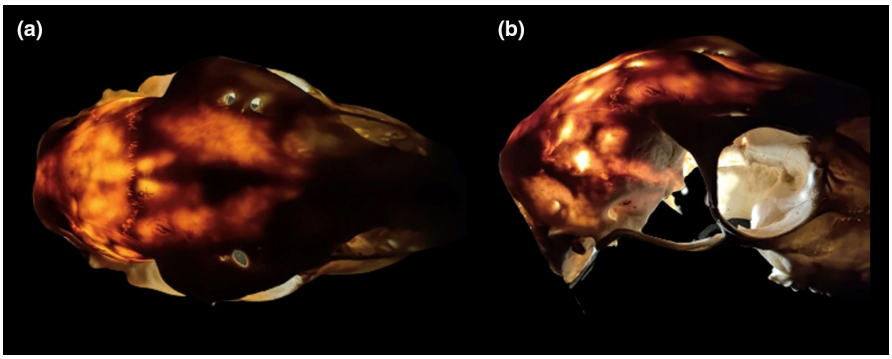

FIGURE 6 Skull of the Patagonian Huemul deer. Transillumination of the cranial cavity. (a) dorsal view; (b) lateral view

worth noting that the hypophyseal fossa of the Patagonian huemul deer was deep and remarkably smooth, similar to what was reported in the roe buck and different to the sheep and goat (Onuk et al., 2013), which could suggest a relevant hypophyseal volume. The number of supraorbital foramina present in the Patagonian huemul deer (two to five per side) was greater than that reported in domestic ruminants (Nickel et al., 1984), reindeer (Castaños, 2017) or pudus (Saldivia & Villegas, 2019). It should be noted that the supraorbital groove extended both rostrally and caudally to the supraorbital foramina, similar to the roe deer (Onuk et al., 2013). In sheep and goats, it is oriented towards the supraorbital foramen (König & Liebich, 2005; Nickel et al., 1984). This suggests that the Patagonian huemul deer present a greater number of nerve branches associated with these structures, as has been described in the roe buck (Onuk et al., 2013). Therefore, the number of supraorbital foramina could be an element to consider during surgical procedures or local anaesthesia (Audisio et al., 2011). On the other hand, in ruminants, during the exploration of the infraorbital nerve as part of the regional anaesthesia procedure, the facial tuberosity is the bone eminence most frequently used as a reference point (*N. infraorbitalis*; Audisio et al., 2011; Clarke & Trim, 2013; Hall et al., 2000; Yalçin & Lök, 2009). Given the absence of facial tuberosity in the Patagonian huemul deer, it is pertinent to palpate the infraorbital foramen, which houses the infraorbital nerve and its branches. Therefore, we suggest using a point located 1 cm dorsally from the alveolar margin of the second premolar as an anatomical landmark.

4.3 | Ecology-related aspects

The bones of the cranium and facies were thin. This was evidenced by some skulls being translucent (Figure 6). However, one aspect that drew attention was the difference in the thickness of the bones between skulls. Although homogeneity was observed between the bones of the same skull, the same did not occur in the analysis between skulls. This suggests a possible unequal nutritional food chain among the geographic places where the populations to which the specimens studied belonged (Escobar et al., 2020; Flueck, 2015, 2018, 2020; Flueck & Smith-Flueck, 2017, 2018, 2020; Smith-Flueck et al., 2018). Another noteworthy aspect was the high number of parietotemporal foramina (from 5 to 16 per side) and those of the temporal squama (from 0 to 3 per side) observed in the Patagonian huemul deer. Generally, these tend to be associated with a high requirement of irrigation and drainage from the cavity (Fandos & Orueta, 1991).

4.4 | Age and sexual dimorphism

The spheno-occipital and intersphenoid synchondrosis have been observed only in the 1.5-year-old skull and associated with the absence of the complete eruption of the third molar is evidence that this synchondrosis has not become obliterated. The rest of the skulls studied presented the third molar and the ossification of the spheno-occipital joint. These findings suggest that the obliteration of the spheno-occipital synchondrosis and eruption of the third molar may occur around the same time. With respect to the intersphenoid synchondrosis, only the 7-year-old skull presented characteristics suggestive of ossification, which suggests that this may be associated with the dolichocephalic skull of the Patagonian huemul deer, because, on the contrary, premature ossification has been reported in brachycephalic canines (Geiger & Haussman, 2016). The 1.5-year-old male, according to the craniometric indices, presented a wide facies and cranium in relation to the other skulls studied. This suggests a bone development that transits phenotypically from a narrow to wide face and skull in the young and the adult, respectively. This could be explained by considering that as the animal develops from fawn to adult, it requires a more elongated and thinner skull shape, while it simultaneously modifies its feeding (Escobar et al., 2020; Iriarte et al., 2017). In Patagonian huemul deer skulls, there was a sexual dimorphism, mainly due to the presence (male) and absence (female) of antlers and pedicles that support them in the frontal bone (Escobar et al., 2020; Iriarte et al., 2017). On the other hand, the female skull presented a greater number (36) of parietotemporal foramina and those in the temporal fossa, associated with a larger diameter. This background is to be expected, since it has been reported that the variability between the number and size of the foramina in the skull of male and female cervids may be due to the type of mechanical load given by the presence or not of antlers (Fandos & Orueta, 1991).

The results of study allow us to propose ecomorphological studies, such as the characterization of the adaptive relation between the morphology of the Patagonian huemul deer and the ecological role that it fulfils in its community, studies of the relation between anatomy and function with aspects of its surroundings to understand the relevance of the bone structures and how these would influence their diet, movement and defence. On the other hand, although the low number of skulls used was an obstacle to the study, we think that the results reported are valid. One piece of information to consider in research on the species is that the laws in Chile and Argentina make it considerably difficult to access biological material for analysis and study, thereby limiting anatomical knowledge. Another limiting aspect was the existence of a terminological void regarding some structures. This is because the NAV is specific to domestic species (ICVGAN, 2017). Although most of the structures observed in the skull are consistent with what was reported in the NAV, there were some that, although they were described, it was not possible to name them.

In conclusion, it may be stated that the Patagonian huemul deer presents an elongated head, extremely elongated cranium and avery narrow facies. The skull presented thin bones, particularly those that form the walls of the cranial cavity, suggesting chronic metabolic imbalances as a response to mineral deficiency. This would reinforce the hypothesis of nutritional deficiency caused by the displacement brought about by human settlements as the main cause of the extinction of the Patagonian huemul deer. In addition to the presence

of two lacrimal foramina, a lacrimal fossa and a preorbital vacuity, there are additional bony eminences that can be used as criteria for the identification of the Patagonian huemul deer skull, such as the location of the styloid process, the caudal projection of the vomerine crest, the absence of the facial tubercle and the presence of the craniopharyngeal canal.

AUTHORS' CONTRIBUTION

Study conception and anatomical description were performed by Samuel Núñez-Cook and Paulo Salinas. Data collection and the first draft of the manuscript was written by Samuel Núñez-Cook. All authors contributed to data analysis, discussion and approved the final manuscript. Paulo Salinas was responsible for supervision of study.

ACKNOWLEDGEMENT

The authors acknowledge the support of PUCV-DI 039.407/2021 (PS) Innovative Interdisciplinary Research.

CONFLICT OF INTEREST

The authors declare no conflicts of interest.

DATA AVAILABILITY STATEMENT

The data that support the findings of this study are available from the corresponding author upon reasonable request.

ORCID

Samuel Núñez-Cook https://orcid.org/0000-0003-3778-6812
Paulo Salinas https://orcid.org/0000-0003-2273-0904

REFERENCES

Arcos, M. A. (2021). *Caracterización fenotípica y sanitaria del Tapetí (Silvilagusbrasiliensis) del cerro El Iguán. provincia del Carchi* [Master's thesis—Universidad Técnica de Cotopaxi], Latacunga, Ecuador. Universitaria UTC. https://repositorio.utc.edu.ec/handle/27000/7619

Audisio, S. A., Vaquero, P. G., Torres, P. A., & Verna, E. C. (2011). *Prevención, manejo y tratamiento del dolor quirúrgico* (1st ed.). Universidad Nacional de La Pampa.

Black-Decima, P. A., Corti, P., Díaz, N., Fernandez, R., Geist, V., Gill, R., Gizejewski, Z., Jiménez, J., Pastore, H., Saucedo, C., & Wittmer, H. (2016). *Hippocamelus bisulcus*. In *The IUCN Red List of Threatened Species*. International Union for Conservation of Nature and Natural Resources e.T10054A22158895.

Brinkschulte, M., Bienert-Zeit, A., Lüpke, M., Hellige, M., Staszyk, C., & Ohnesorge, B. (2013). Using semi-automated segmentation of computed tomography datasets for three-dimensional visualization and volume measurements of equine paranasal sinuses. *Veterinary Radiology & Ultrasound*, *54*(6), 582–590. https://doi.org/10.1111/vru.12080

Cabrera, A. (1941). Cranial and dental characters of some south American Cervidae. *Field Museum of Natural History, Chicago*, *27*, 125–135.

Castañeda, H., Navarrete, N., Sato, A., & Chávez, A. (2016). Osteometría del cráneo de la alpaca adulta (*Vicugna pacos*). *Revista de InvestigacionesVeterinarias del Perú*, *27*(3), 403–420. https://doi.org/10.15381/rivep.v27i3.11992

Castaños, J. (2017). *Grandes faunas esteparias del Cantábrico oriental estudio isotópico y paleontológico de los macrovertebrados del pleistoceno superior de kiputzix (Mutriku, gipuzkoa)* (1st ed.). KOBIE.

Clarke, K. W., & Trim, C. M. (2013). *Veterinary anaesthesia e-book* (1st ed.). Elsevier Health Sciences.

Clauss, M., Hofmann, R. R., Streich, W. J., Fickel, J., & Hummel, J. (2008). Higher masseter muscle mass in grazing than in browsing ruminants. *Oecologia*, *157*(3), 377–385. https://doi.org/10.1007/s00442-008-1093-z

Coacalla, C. Z., Curie, J. I. P., & Flores, J. C. A. (2021). Descripción osteológica de la taruca (*Hipocamelusantisensis*) (d'Orbigny, 1834): II. Esqueleto axial. *Revista de Investigaciones Veterinarias del Perú*, *32*(6), e21703. https://doi.org/10.15381/rivep.v30i2.16096

Escobar, M., Smith, J. M., & Flueck, W. T. (2020). *El Huemul: Shoonem, Madera que se mueve/re* (2nd ed.). Biblioteca Popular "Dr. Enrique Perea".

Fandos, P., & Orueta, F. (1991). Variaciones morfológicas en el cráneo del corzo (*Capreolus capreolus* L). *Doñana Acta Vertebrata*, *18*(2), 159–171.

Fedorov, A., Beichel, R., Kalpathy-Cramer, J., Finet, J., Fillion-Robin, J. C., Pujol, S., Bauer, C., Jennings, D., Fennessy, F., Sonka, M., Buatti, J., Aylward, S. R., Miller, J. V., Pieper, S., & Kikinis, R. (2012). 3D slicer as an image computing platform for the quantitative imaging network. *Magnetic Resonance Imaging*, *30*(9), 1323–1341.

Flueck, W. T. (2015). Osteopathology and selenium deficiency co-occurring in a population of endangered Patagonian huemul (*Hippocamelus bisulcus*). *BMC Research Notes*, *8*(1), 330. https://doi.org/10.1186/s13104-015-1291-9

Flueck, W. T. (2018). Elusive cranial lesions severely afflicting young endangered Patagonian huemul deer: A case report. *BMC Research Notes*, *11*(1), 638. https://doi.org/10.1186/s13104-018-3755-1

Flueck, W. T. (2020). Nutrition as an etiological factor causing diseases in endangered huemul deer. *BMC Research Notes*, *13*(276), 1–12. https://doi.org/10.1186/s13104-020-05122-1

Flueck, W. T., & Smith-Flueck, J. M. (2008). Age-independent osteopathology in skeletons of a South American cervid, the Patagonian huemul (*Hippocamelus bisulcus*). *Journal of Wildlife Diseases*, *44*(3), 636–648. https://doi.org/10.7589/0090-3558-44.3.636

Flueck, W. T., & Smith-Flueck, J. M. (2011). Osteological comparisons of appendicular skeletons: A case study on Patagonian huemul deer and its implications for conservation. *Animal Production Sciences*, *51*(4), 327–339. https://doi.org/10.1071/AN10174

Flueck, W. T., & Smith-Flueck, J. M. (2017). Troubling disease syndrome in endangered live Patagonian huemul deer (*Hippocamelus bisulcus*) from the Protected Park Shoonem: Unusually high prevalence of osteopathology. *BMC Research Notes*, *10*, 739. https://doi.org/10.1186/s13104-017-3052-4

Flueck, W. T., & Smith-Flueck, J. M. (2018). Radio marking the first group of endangered Patagonian huemul deer in Argentina. *Mastozoologia Neotropical*, *25*(2), 461–565. https://doi.org/10.31687/saremMN.18.25.2.0.07

Flueck, W. T., & Smith-Flueck, J. M. (2020). The next frontier for recovering endangered huemul (*Hippocamelus bisulcus*): How to avoid recurrent misdiagnoses of health status and risks. *Animal Production Sciences*, *60*(10), 1271. https://doi.org/10.1071/AN18688

Geiger, M., & Haussman, S. (2016). Cranial suture closure in domestic dog breeds and its relationships to skull morphology. *Anatomical Record*, *299*(4), 412–420. https://doi.org/10.1002/ar.23313

Gündemir, O., Duro, S., Jashari, T., Kahvecioğlu, O., Demircioğlu, İ., & Mehmeti, H. (2020). A study on morphology and morphometric parameters on skull of the Bardhoka autochthonous sheep breed in Kosovo. *Anatomia, Histologia, Embryologia*, *49*(3), 365–371.

Hall, L. W., Clarke, K. W., & Trim, C. M. (2000). *Wright's veterinary anaesthesia and analgesia* (10th ed.). ELBS and Bailliere Tindall.

Heckeberg, N. S. (2020). The systematics of the Cervidae: a total evidence approach. *PeerJ*, *8*, e8114. https://doi.org/10.7717/peerj.8114

International Committee on Veterinary Gross Anatomical Nomenclature. (2017). *Nomina Anatomica Veterinaria* (6th ed.). Editorial Committee Hanover (Germany).

Iriarte, A., Donoso, D. S., Segura, B., & Tirado, M. (2017). *El Huemul de Aysén y otros rincones* (1st ed.). Ediciones Secretaría Regional Ministerial de Agricultura de la Región de Aysén y Flora & Fauna Chile Limitada.

Keneisenuo, K., Choudhary, O. P., Kalita, P. C., Choudhary, P., Kalita, A., Doley, P. J., & Chaudhary, J. K. (2021). Comparative morphometrical studies on the skull bones of barking deer (Muntiacus muntjak) and sambar deer (*Rusa unicolor*). *Anatomia, Histologia, Embryologia*, *50*(3), 500–511.

König, H., & Liebich, H. (2005). *Anatomía de los Animales Domésticos, Tomo 1* (2nd ed.). Madrid, España. Médica Panamericana.

Krenzer, U. (2006). *Compendio de métodos antropológicos forenses para la reconstrucción del perfil osteo-biológico Tomo 1: osteometría* (1st ed.). Serie de Antropología Forense.

Mateo, A. G., & Sánchez, H. L. (2016). Descripción anatómica de los músculos masticadores de un ciervo axis (*Axis axis*). *Analecta Veterinari*, *36*(1), 25–29.

Merino, M. L., Milne, N., & Vizcaíno, S. F. (2005). A cranial morphometric study of deer (Mammalia, Cervidae) from Argentina using three-dimensional landmarks. *Acta Theriologica*, *50*, 91–108.

Nickel, R., Schummer, A., Seiferle, E., Frewein, J., Wille, K. H., & Wilkens, H. (1984). *Lehrbuch der anatomie der haustiere I: Bewegungs apparat* (5th ed.). Verlag Paul Parey.

Núñez, F. E. (2018). *Caracterización Morfológica del Lagomorfo Silvestre Ecuatoriano en la Provincia de Cotopaxi* [Bachelor's thesis—Universidad Técnica de Cotopaxi]. Latacunga, Ecuador. Universitaria UTC. https://repositorio.utc.edu.ec/handle/27000/5384

Onuk, B., Kabak, M., & Atalar, K. (2013). Anatomic and craniometric factors in differentiating roe deer (*Capreolus capreolus*) from sheep (*Ovis aries*) and goat (*Capra hircus*) skulls. *Archives of Biological Sciences*, *65*(1), 133–141. https://doi.org/10.2298/ABS1301141M

Pohlmeyer, K. (1985). *Zur vergleichenden Anatomie von Damtier, Schaf und Ziege. Osteologie und postnatale Osteogenese* (1st ed.). Verlag Paul Parey.

Riquelme, C., Estay, S. A., López, R., Pastore, H., Soto-Gamboa, M., & Corti, P. (2018). Protected areas' effectiveness under climate change: A latitudinal distribution projection of an endangered mountain ungulate along the Andes Range. *PeerJ*, *6*, e5222. https://doi.org/10.7717/peerj.5222

Rolfe, S., Pieper, S., Porto, A., Diamond, K., Winchester, J., Shan, S., Kirveslahti, H., Boyer, D., Summers, A., & Maga, A. M. (2021). SlicerMorph: An open and extensible platform to retrieve, visualize and analyse 3D morphology. *Methods in Ecology and Evolution*, *12*(10), 1816–1825. https://doi.org/10.1111/2041-210X.13669

Saldivia, M., & Villegas, F. (2019). Descripción anatómica de los segmentos óseos que componen el cráneo de la especie *Pudu puda*. *International Journal of Morphology*, *37*(1), 167–173. https://doi.org/10.4067/S0717-95022019000100167

Salinas, P., Arenas-Caro, A., Núñez-Cook, S., Moreno, L., Curihuentro, E., & Vidal, F. (2020). Morphometric, anatomic and radiographic study of bone of the pelvic limb of endangered Patagonian huemul deer (*Hippocamelus bisulcus*). *International Journal of Morphology.*, *38*(3), 747–754. https://doi.org/10.4067/S0717-95022020000300747

Salinas, P., Núñez-Cook, S., Arenas-Caro, A., Moreno, L., Curihuentro, E., & Vidal, F. (2020). Anatomy, morphometry and radiography in the thoracic limb bones of the Patagonian huemul deer (*Hippocamelus bisulcus*). *Anatomia, Histologia, Embryologia*, *49*(4), 494–501. https://doi.org/10.1111/ahe.12553

Sandoval, R. S., Ruiz, L. F., Salinas, E. A., & Victorio, W. M. (2016). Craneotomía Rostrotentorial Descompresiva en un Carnero Reproductor. *Revista de Investigaciones Veterinarias del Perú*, *27*(4), 826–832. https://doi.org/10.15381/rivep.v27i4.12577

Sañudo, C. (2009). *Valoración morfológica de los animales domésticos* (1st ed.). Ministerio de Medio Ambiente y Medio Rural y Marino, Centro de Publicaciones.

Silvestrini, P., Piviani, M., & Ruiz de Gopegui, R. (2008). Enanismo hipofisario congénito en un gato siamés. *Clínica veterinaria de pequeños animales*, *28*(3), 169–172.

Simmons, J. E., & Muñoz-Saba, Y. (2005). *Conservación Internacional Serie manuales para la conservación I: Cuidado, manejo y conservación de las colecciones biológicas* (1st ed.). Universidad Nacional de Colombia.

Smith-Flueck, J., Flueck, W. T., & Escobar, M. (2018). Preliminary data on movements and health condition of the first radio-collared huemul (*Hippocamelus bisulcus*) population study in Argentina. *DSG Newsletter*, *30*, 4–14.

Von den Driesch, A. (1976). *A guide to the measurement of animal bones from archaeological sites: As developed by the Institut für Palaeoanatomie, Domestikationsforschung und Geschichte der Tiermedizin of the University of Munich* (Vol. *1*). Peabody Museum Press.

Wemmer, C. M., & Wilson, D. E. (1987). Cervid brain size and natural history. In C. M. Wemmer (Ed.), *Biology and management of the Cervidae*. Smithsonian Institution Press.

Yahaya, A., Olopade, J. O., & Kwari, H. D. (2011). Clinical implications of craniometric indices of the one-humped camel (*Camelus dromedarius*) to oral health and clinical regional anaesthesia of the head. *Journal of Veterinary Anatomy*, *4*(1), 19–31. https://doi.org/10.21608/jva.2011.45166

Yalçin, H., & Lök, S. (2009). Anadolu Yaban Koyunu (Ovis gmelini anatolica) ve Akkaraman Koyununun (Ovis aries) Kafa Kemikleri Üzerinde Karşilaştirmali Makro-Anatomik Araştirma. *Atatürk University Journal of Veterinary Sciences*, *4*(3), 147–162.

SUPPORTING INFORMATION

Additional supporting information can be found online in the Supporting Information section at the end of this article.

How to cite this article: Núñez-Cook, S., Vidal Mugica, F., & Salinas, P. (2022). Skull anatomy of the endangered Patagonian huemul deer(*Hippocamelus bisulcus*). *Anatomia, Histologia, Embryologia*, *00*, 1–12. https://doi.org/10.1111/ahe.12851